Coherent control of Fano resonances in a macroscopic four-mirror cavity

Nikhil Pramanik,[1] K. C. Yellapragada,[2] Suneel Singh,[1] and P. Anantha Lakshmi[1,*]
[1]*School of Physics, University of Hyderabad, Hyderabad, Telangana 500046, India*
[2]*Centre for Quantum Technologies, 3 Science Drive 2, National University of Singapore, 117543 Singapore, Singapore*

(Received 3 May 2019; revised manuscript received 20 December 2019; accepted 3 February 2020; published 1 April 2020)

We demonstrate coherent control of optomechanically induced transparency and Fano resonances in a four-mirror macroscopic optomechanical cavity, with two movable mirrors, each driven by an external mechanical pump. The variable control of the amplitude and phase of the coherent mechanical pumps provides a means of tuning the shape and nature of the Fano profiles. Further, our scheme shows the occurrence of tunable optomechanical features, even at very low mechanical driving field amplitudes, in macroscopic optomechanical cavities.

DOI: 10.1103/PhysRevA.101.043802

I. INTRODUCTION

Quantum interference between different transition pathways gives rise to several interesting physical phenomena, such as Fano resonances [1,2], that have been observed in a variety of physical systems. For instance, in plasmonics, photons are allowed to travel through multiple transition pathways which interfere, thus making the occurrence of Fano line shapes quite common in such materials. Fano resonances have been observed in a wide variety of systems which include the phonon interactions in solids [3,4]; electron transport in quantum wells, quantum dots [5,6], and three-dimensional waveguides [7]; coupled photonic microcavities [8,9]; plasmonic metamaterials [10,11] and nanostructures [12–15]; and photonic materials [16–20].

Fano line shapes have also been used in obtaining information on the interaction between a wide variety of nanostructures with light [21], for local refractive index sensing applications [22], efficient confinement of light [23], surface-enhanced Raman scattering [24], generation of slow light in metamaterials [25], enhanced light transmission [26], and sensitive biosensors [27]. Fano interference is seen to play an important role in producing a strong cooling effect in a Michelson-Sagnac interferometer [28], in lasing without population inversion [29–32], and as a tool to probe decoherence [33,34] in the field of quantum optics and quantum information. More recently, Fano resonances have been widely studied theoretically in hybrid optomechanical systems with distinct configurations involving double cavities [35], whispering gallery modes [36], BEC [37,38], and two-level atoms and qubits [39,40], to name a few. The regulation of Fano line shapes in an optomechanical (OM) cavity is observed by applying an external magnetic field [41]. Piao *et al.* [42–44] proposed a new mechanism focused on the spin-dependent separation of Fano resonance spectra for the nonmagnetic achievement of optical spin angular momentum. A detailed analysis of Fano resonances and the generation of slow light was carried out in Refs. [37,39,45].

Fano interference leading to destructive interference of quantum noise can be used to cool the mechanical oscillator close to its ground state [46]. Plasmonic-metal–dielectric-metal stub structures show the presence of Fano-type spectral asymmetry in its transmittance spectra which is used in a plasmonic waveguide modulator [42,43,47]. Spin-dependent Fano resonances lead to spectral separation of optical spin angular momentum [44]. In mesoscopic scales efficient Fano resonance control has been shown in a quantum dot in an Aharonov-Bohm interferometer [48].

In conventional optomechanical systems, the OM effects can be detected for sufficiently strong coupling strengths, with the coupling parameter defined as G, which requires extremely small sizes of mirrors and cavity arm lengths. In macroscopic cavities, due to their dimensions, the OM coupling G is very weak and hence the ensuing OM effects are not detectable. In this work we propose a scheme to observe the OM effects even in macroscopic cavities by introducing coherent mechanical drive on the mirrors. More specifically, we study the occurrence of Fano resonances and the related phenomenon of optomechanically induced transparency (OMIT) [49], from a study of the generated anti-Stokes signals in a macroscopic cavity. The cavity here is operating in the dark-mode configuration that is commonly used in LIGO interferometers [50]. A basic four-mirror nanomechanical system was studied by Farman and Bahrampour [51], in which they reported the existence of Fano resonances. In the present work, we have modified their system by adding hybrid elements, and more importantly, we have looked at the performance of the system at the macroscopic level, which gives an entirely new perspective of the system behavior. For instance, the current study reveals that the introduction of mechanical pumping enhances the optomechanical interaction significantly, resulting in the appearance of Fano resonances and OMIT in the generated anti-Stokes signals. Further, externally pumping

*palsp@uohyd.ernet.in

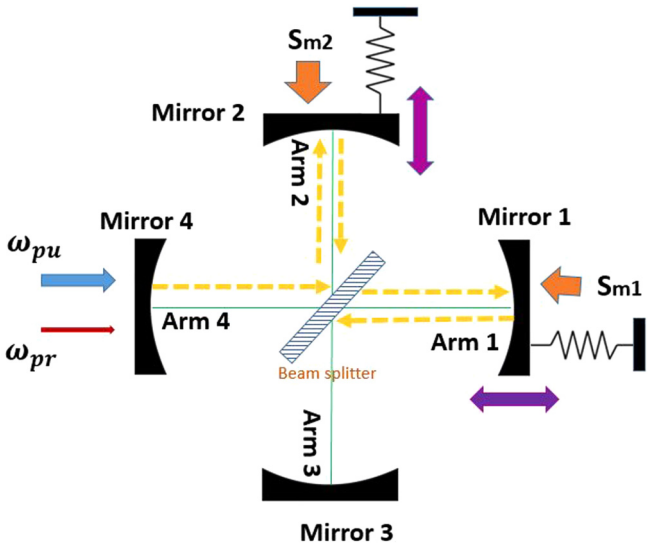

FIG. 1. Schematic diagram of a four-mirror cavity with two movable mirrors.

the two independently oscillating mirrors provides a handle, in terms of the mechanical pump's amplitude and phase, to control the resonances, which has been explored in great detail in the present study. For an appropriate choice of the amplitude and the phase of the mechanical driving fields, the system exhibits tunable double Fano resonances. This work, involving a detailed study of the macroscopic hybrid four-mirror system, assumes relevance from the experimental point of view, viz., in the LIGO observatory.

The paper is organized as follows: In Sec. II a detailed description of the system that is studied here is provided, together with necessary mathematical formulation and solutions for the dynamical evolution of different quantities of interest. In Sec. III numerical results pertaining to the OMIT and the asymmetric Fano-like resonance induced by interference of two transition pathways are presented. We further show the generation of double Fano-like resonances for specific choices of the drive amplitudes and phases. A summary of the results and the conclusions are presented in Sec. IV.

II. MODEL AND THEORY

Figure 1 shows a schematic of the four-mirror cavity considered in this work. Mirrors 1 and 2 are movable, each of which are driven by a coherent mechanical pump, while mirrors 3 and 4 are fixed. A pump laser of frequency $\omega_{\rm pu}$ and a probe laser of frequency $\omega_{\rm pr}$ enter the cavity from the left. The frequency of the cavity is taken to be ω_0. In this study, we consider the dark-mode configuration as is commonly employed in LIGO studies [50], wherein destructive interference leads to no field in arm 3, which is nonresonant with the field [52,53]. However any imperfections in destructive interference that may result in photon loss, which may occur due to a slight leakage of photons into arm 3, are incorporated through the cavity decay rate κ.

The Hamiltonian, describing the various interactions that are considered here, is written in a rotating frame with frequency ω_0 as follows:

$$\begin{aligned} H =& \hbar\Delta_c a^\dagger a + \sum_{i=1,2} \frac{\hbar\omega_{mi}}{2}\left(P_i^2 + Q_i^2\right) - \hbar \sum_{i=1,2} G_i a^\dagger a Q_i \\ &+ i\hbar\epsilon_{pu}(a^\dagger - a) + i\hbar\epsilon_{pr}(a^\dagger e^{-i\delta t} - a e^{i\delta t}) \\ &- \sum_{i=1,2} S'_{mi} Q_i \cos(\delta t + \phi_{mi}). \end{aligned} \tag{1}$$

Here a and $a^\dagger$ are the bosonic operators of the cavity field, and P_i and Q_i are the momentum and position operators of the two movable mirrors, each of which are modeled as simple harmonic oscillators, with frequency ω_{mi}, effective mass m_i, and mechanical decay rate γ_i, with i taking the values 1 and 2. The pump (probe) amplitude $\epsilon_{\rm pu}$ ($\epsilon_{\rm pr}$) is related to the input pump (probe) power $P_{\rm pu}$ ($P_{\rm pr}$) as $\epsilon_{\rm pu} = \sqrt{2\kappa P_{\rm pu}/\hbar\omega_{\rm pu}}$ ($\epsilon_{\rm pr} = \sqrt{2\kappa P_{\rm pr}/\hbar\omega_{\rm pr}}$). The optomechanical coupling rate is given by $G_i = \frac{\omega_c}{L_i}\sqrt{\hbar/m_i\omega_{mi}}$ ($i = 1$ and 2) [52,53], where L_i is the length of the cavity. The first term describes the cavity field energy with the cavity detuning given by $\Delta_c = \omega_0 - \omega_{\rm pu}$, and the second term is the energy of the two mechanical oscillators. The third term describes the optomechanical interaction arising due to the coupling between the two mechanical oscillators and the cavity field. The fourth and fifth terms describe the interaction between the cavity field and the input pump and probe fields, respectively, with $\delta = \omega_{\rm pr} - \omega_{\rm pu}$, the pump-probe detuning. The last term describes the mechanical pumping energy applied to each movable mirror, with the driving parameter S'_{mi} defined by $S'_{mi} = s_{mi}\sqrt{\hbar/m_i\omega_{mi}}$ ($i =$ 1 and 2), where the quantities s_{mi} and ϕ_{mi} ($i = 1$ and 2) are the amplitude and the phase of the coherent mechanical drive.

We denote the expectation values of each of the operators $\hat{a}$, $\hat{Q}$, and $\hat{P}$ with $\langle a\rangle$, $\langle Q\rangle$, and $\langle P\rangle$, respectively. Using the Hamiltonian given in Eq. (1), we derive the equations that describe the dynamical behavior of these operator expectation values in the Heisenberg picture as follows:

$$\begin{aligned} \frac{d\langle a\rangle}{dt} =& -i\Delta_c\langle a\rangle + \epsilon_{\rm pu} + \epsilon_{\rm pr}e^{-i\delta t} + iG_1\langle a\rangle\langle Q_1\rangle \\ &+ iG_2\langle a\rangle\langle Q_2\rangle - \kappa\langle a\rangle, \\ \frac{d\langle Q_i\rangle}{dt} =& \omega_{mi}\langle P_i\rangle \quad (i = 1, 2), \\ \frac{d\langle P_i\rangle}{dt} =& -\omega_{m1}\langle Q_i\rangle + G_i\langle a^\dagger\rangle\langle a\rangle - \gamma_i\langle P_i\rangle \\ &+ \frac{S'_{mi}}{\hbar}cos(\delta t + \phi_{mi}) \quad (i = 1, 2). \end{aligned} \tag{2}$$

In the above equations, κ is the cavity decay rate. In obtaining the above equations of motion, the mean-field assumption $\langle MN\rangle = \langle M\rangle\langle N\rangle$ for the relevant operators has been used. Next, each of the variables is separated into a steady-state solution and a small fluctuation around its steady-state value, i.e., $\hat{x} = x_s + \delta\hat{x}$. By substituting the same in each of the above equations, we can obtain the steady-state solutions [Eq. (A1)] as well as the equations of motion for the fluctuations in each of these operators. A detailed derivation of these is given in the Appendix.

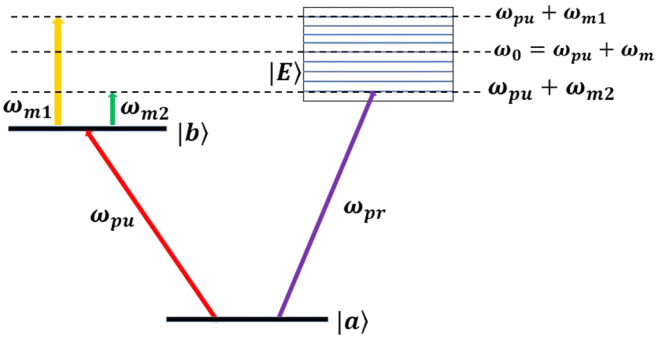

FIG. 2. Schematic illustration of frequencies used in obtaining Fano line shapes.

To study the absorption characteristics of the OM system we have to obtain an expression for the following anti-Stokes component of the output field from the cavity:

$$\mathrm{Re}(\eta_{\mathrm{as}}) = \mathrm{Re}(2\kappa a_1^-/\epsilon_{\mathrm{pr}}). \tag{3}$$

The resulting equations for the fluctuations in relevant variables are obtained, details of which are provided in the Appendix. These equations are solved analytically to obtain the final form of the component a_1^- given by

$$a_1^- = \frac{\epsilon_{\mathrm{pr}} + iG_1 a_s Q_1^- + iG_2 a_s Q_2^-}{\kappa + i(\Delta - \delta)}, \tag{4}$$

where the expressions for Q_1^- and Q_2^- are given in the Appendix. Here a_1^- is the transition amplitude, which contains the interfering contributions arising from the anti-Stokes component of the scattered light and the incident probe field. The anti-Stokes component arises due to absorption of a phonon from the mirror, thus leading to cooling of the mirror [35]. As shown in Fig. 2, when the pump field of the frequency ω_{pu} interacts with the mechanical mirror of frequency, say, Ω, absorption and emission of phonons create the anti-Stokes field ($\omega_{\mathrm{pu}} + \Omega$) and the Stokes field ($\omega_{\mathrm{pu}} - \Omega$), respectively [54]. If the frequency of the pump laser is red-detuned (tuned below the resonance frequency of the cavity exactly by an amount Ω), then the anti-Stokes field becomes resonant with the cavity field and therefore gets enhanced, at the cost of suppression of the Stokes field, as now the Stokes field is far removed from resonance.

Fano, in a seminal paper [1], first described the asymmetric profile resulting in Rydberg spectral atomic lines and provided a detailed explanation of this feature arising due to resonant destructive interference between two transition pathways. In particular, one observes a minimum with an accompanying maximum very close to it, which is known by the name Fano resonance. Inside the four-mirror cavity, when the frequency of the probe beam is tuned to that of the generated anti-Stokes field, destructive interference between these two fields gives rise to a Fano-like resonance. As shown in Fig. 2, interference takes place between the two transition pathways $|a\rangle \rightarrow |E\rangle$ and $|a\rangle \rightarrow |b\rangle \rightarrow |E\rangle$, where $|E\rangle$ represents a continuum of states. Thus, when $\omega_{\mathrm{pr}} = \omega_{\mathrm{pu}} + \omega_{m1}$, destructive interference between the two fields (anti-Stokes and the probe) leads to a Fano-like resonance. The availability of two oscillating mirrors, which can be tuned independently of each other, at frequencies ω_{m1} and ω_{m2}, respectively, provides two transition pathways from state $|b\rangle$ to the continuum $|E\rangle$. A suitable choice of these parameters gives rise to a double Fano-like resonance. For instance, choosing the mechanical oscillation frequency of both the mirrors to be equal ($\omega_{m1} = \omega_{m2}$) results in superposition of the two resonances. Under this condition, the resulting Fano-like profile can be modified, giving rise to interesting features, by tuning the amplitude and the phase of the coherent mechanical pump. These features are illustrated in the figures presented in the next section.

In the next section we present numerical simulations of the results for the real part of the generated anti-Stokes field as a function of the normalized probe detuning $\delta_{\mathrm{pr}}/\Omega$, where $\delta_{\mathrm{pr}} = \omega_{\mathrm{pr}} - \omega_0$, for a wide range of parameters, and we present a discussion of the results.

III. RESULTS AND DISCUSSION

In this study, we have considered a truly macroscopic four-mirror cavity, with the following parameters. The length of each cavity is $L_i = 70$ mm ($i = 1,2$), the effective pump laser detuning is $\Delta = \Omega = 2\pi \times 10^7$ Hz, the cavity decay rate is $\kappa = 2\pi \times 10^6$ Hz, the mechanical damping rate of each movable mirror is $\gamma_{mi} = 2\pi \times 10^4$ Hz ($i = 1$ and 2), the mass of each mirror is $m_i = 145$ mg, ($i = 1$ and 2), the wavelength of the pump laser is $\lambda = 1064$ nm, and the pump power $P_{\mathrm{pu}} = 10$ μW. It is to be noted that the parameters used in this study have been obtained from a careful survey of existing literature on macroscopic hybrid optomechanical systems [55–64]. Due to the macroscopic nature of the parameters of the four-mirror setup, the optomechanical coupling is too weak to show any observable optomechanical effects such as the optomechanically induced transparency and the Fano resonances which were earlier reported in microscopic cavities [35,51]. This problem can, however, be circumvented by the application of a very nominal coherent driving field, resulting in observable optomechanical effects. In the following, we present numerical results for the real part of the anti-Stokes field for a variety of parameters, the details of which are contained in each of the figures, and demonstrate the significant role played by the amplitude and the phase of the coherent mechanical drive in observing the interesting features reported here.

In the analytical expressions that were obtained in the previous section, the optomechanical interaction terms appear to several orders of the coupling parameter G. However, because the present OM system has very weak optomechanical coupling, owing to its macroscopic nature as determined by the parameters that were considered, the quadratic and higher-order terms result in negligible contributions to the features that are observed. We therefore neglect the higher-order optomechanical interaction terms and retain only the linear terms in the interaction strength G. This gives rise to considerable simplification in the expression for a_1^-, which is obtained after neglecting all components containing second- and higher-order terms of effective OM coupling strength G_i ($i = 1$ and 2), as shown below. It is to be noted that the scheme proposed here, involving the coherent mechanical driving of the mirrors, enhances the optomechanical interaction giving rise to observable effects, even at very nominal mechanical

driving amplitudes s_{mi} ($i = 1$ and 2):

$$a_1^- = \frac{\epsilon_{\rm pr} + iG_1 a_s S_{m1}\chi_1(\delta)e^{-i\phi_{m1}} + iG_2 a_s S_{m2}\chi_2(\delta)e^{-i\phi_{m2}}}{\kappa + i(\Delta - \delta)}. \tag{5}$$

From the above expression it is clear that the effective coupling strength of the ith cavity is the product of G_i and S_{mi}, which is inversely proportional to the length L_i of the cavity and the mass m_i of the mirror and directly proportional to the mechanical driving amplitude s_{mi}. Hence, as the mirror mass and the cavity length are simultaneously increased, the mechanical driving amplitude also has to be increased in order to detect any discernible effects. The above result can be simplified further for the symmetric cases $G_1 = G_2 = G$ and $\chi_1(\delta) = \chi_2(\delta) = \chi(\delta)$, with the introduction of the parameter $A = iGa_s\chi(\delta)$, resulting in the expression

$$a_1^- = \frac{\epsilon_{\rm pr} + A(S_{m1}e^{-i\phi_{m1}} + S_{m2}e^{-i\phi_{m2}})}{\kappa + i(\Delta - \delta)}. \tag{6}$$

We now examine the structure of the real part of the anti-Stokes field under the conditions $\omega_{m1} = \omega_m$, $\gamma_1 = \gamma$, and $S_{m2} = 0$ (no mechanical pumping of mirror 2) and for a particular value of phase $\phi_{m1} = 3\pi/2$. Further if we define $x = \omega_m - \delta$, then in the vicinity of the resonance where $\delta \simeq \omega_m$ and $\Delta \simeq \Omega$, the real part of the anti-Stokes field can be obtained approximately as

$$\mathrm{Re}(\eta_{\rm as}) \simeq a\,\frac{(q + \bar{x})^2 + b}{\left(\frac{\bar{\gamma}^2}{4}\right) + \bar{x}^2}, \tag{7}$$

which has the general form of the Fano profile in lossy systems (see Eq. (7) of Ref. [65]). In the above equation, $\bar{x} = x/\kappa$, $\bar{\gamma} = \gamma/\kappa$, $\bar{\Omega} = -\Omega/\kappa$, $\tilde{G} = 2GS_{m1}(\epsilon_{\rm pu}/\epsilon_{\rm pr})$, $q = \tilde{G}/4\kappa^2$, $a = \frac{2}{1+\bar{\Omega}^2}$, and $b = (-q^2 + \frac{\bar{\gamma}^2}{4} - \frac{G}{2\kappa^2}\frac{\bar{\gamma}}{\Delta})$.

We now study the behavior of output spectra for various combinations of the amplitudes and phases of the two coherent mechanical pumps. At first, we look at the case when $\phi_{m1} = \phi_{m2} = 3\pi/2$. Taking $\Delta = \delta = \Omega$, it is observed that a phase of $3\pi/2$ gives rise to OMIT at the line center. It is further seen that the strength of the OMIT feature (as quantified by how close the dip is to its zero value) is proportional to the amplitude of the coherent mechanical pump; this is illustrated in Fig. 3(a). The absence of mechanical driving, i.e., $s_{m1} = 0$ (black curve), shows an absence of OMIT at the line center. The introduction of a small driving amplitude of $s_{m1} = 2.6$ mN (red curve) results in a dip at the line center, which indicates transmission of the probe beam on resonance. With further increase in the amplitude, $s_{m1} = 5.6$ mN (blue curve), one observes a complete transmission of the probe beam. The destructive interference between the probe beam and the anti-Stokes field when $\omega_{\rm pr} = \omega_{\rm pu} + \omega_{m1}$ gives rise to OMIT at the line center corresponding to $\omega_{m1} = \Omega$. The results of Fig. 3 show that an increase in the strength of the mechanical pump gives rise to an enhancement in probe transmission, leading to complete transmission (OMIT) for a particular value of this parameter.

In Fig. 3(b), the absence of a dip at the line center in the black curve shows clearly that OM effects are not present when the mechanical driving field is not applied, i.e., $s_{m1} = s_{m2} = 0$. The introduction of a small mechanical pump of amplitude $s_{m1} = 2.7$ mN on mirror 1, with $\omega_{m1} = \Omega$, gives rise to a dip at the line center, as seen in the red curve, showing clearly the generation of OMIT. Further inclusion of a mechanical pump of the same amplitude ($s_{m2} = 2.7$ mN) on mirror 2, with both the phases held at the same value, i.e., $\phi_{m1} = \phi_{m2} = 3\pi/2$, gives rise to complete transparency of the probe beam at the line center (blue curve). This feature can be attributed as arising due to the coherent addition of the OM contributions arising from each of the mechanical driving fields, which are at the same phase.

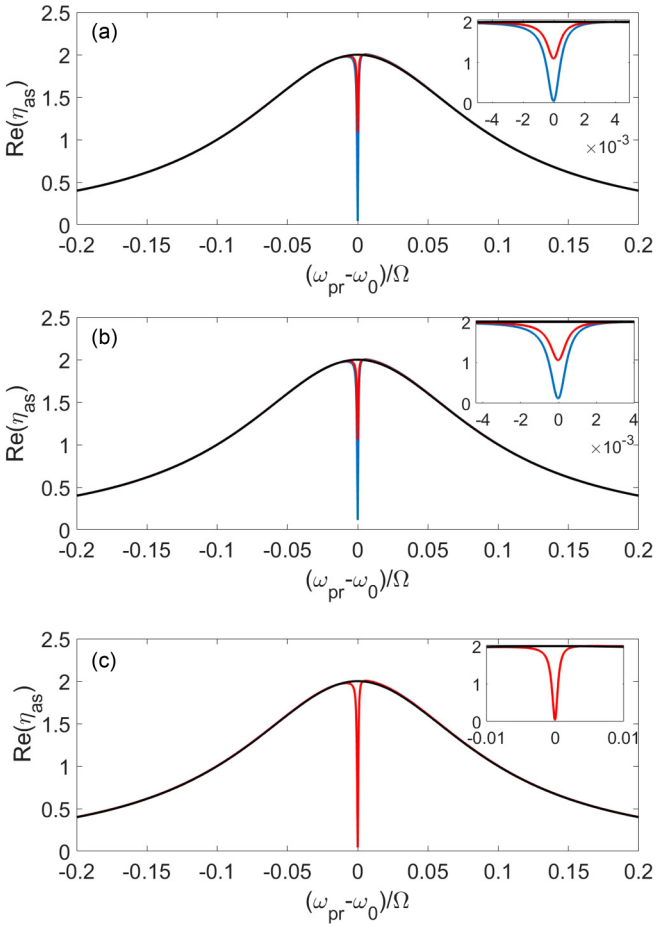

FIG. 3. The real part of the anti-Stokes field as a function of normalized probe detuning for $\omega_{m1} = \Omega$, $\phi_{m1} = 3\pi/2$, and the following parameters: (a) $s_{m1} = 5.6$ mN (blue curves), $s_{m1} = 2.6$ mN (red curves), and $s_{m1} = 0$ and $s_{m2} = 0$ (black curves); (b) $s_{m1} = s_{m2} = 2.7$ mN (blue curves), $s_{m1} = 2.7$ mN and $s_{m2} = 0$ (red curves), and $s_{m1} = s_{m2} = 0$ (black curves); and (c) $s_{m1} = 5.7$ mN and $s_{m2} = 0$ (red curves), and $s_{m1} = s_{m2} = 5.7$ mN and $\phi_{m2} = \pi/2$ (black curves).

This can further be substantiated by exploring whether the effect will be canceled out by tuning one of the mechanical driving fields completely out of phase with the second drive field. This is indeed the case, as shown in Fig. 3(c), where the red curve shows complete transparency of the probe beam at the line center, generated solely due to s_{m1}, at a phase of $\phi_{m1} = 3\pi/2$. Introducing the second mechanical drive s_{m2} at a phase of $\phi_{m2} = \pi/2$ provides another channel which destructively interferes to cancel out this OMIT effect, as can be seen from the black curve. Thus, tuning the amplitude and the phase of

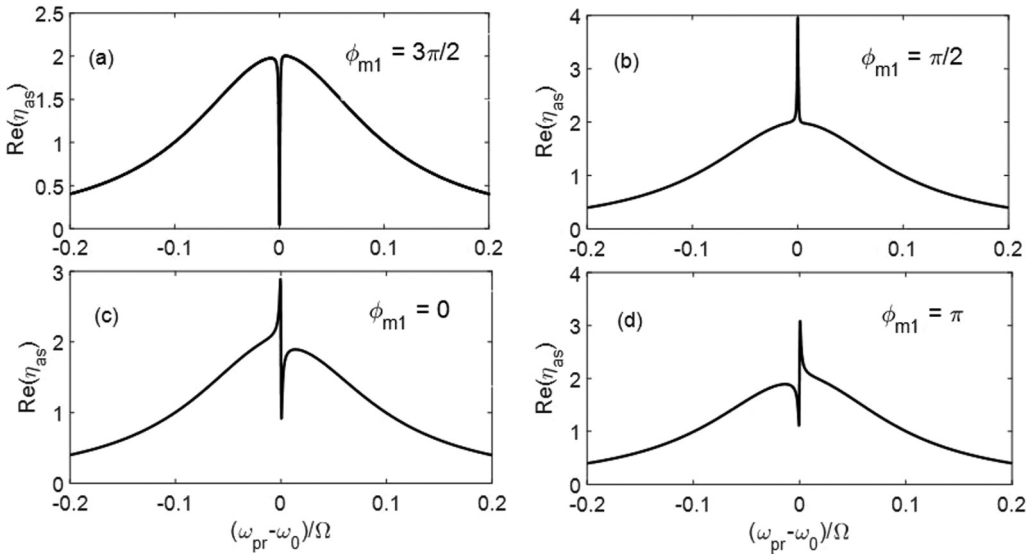

FIG. 4. The real part of the anti-Stokes field as a function of normalized probe detuning for different values of phase ϕ_{m1}. (a) $\phi_{m1} = 3\pi/2$. (b) $\phi_{m1} = \pi/2$. (c) $\phi_{m1} = 0$. (d) $\phi_{m1} = \pi$.

the coherent mechanical pumps gives a handle to control the generation of OMIT in a macroscopic cavity.

In the results presented so far, it has been shown that OMIT is observed at the line center, when the phases of the mechanical driving fields are held at $3\pi/2$. It would be interesting to see the effect of varying the phase of the mechanical pump on the OMIT features. For this purpose, first, we switch off one of the mechanical pumps, say $s_{m2} = 0$, and keep the amplitude s_{m1} fixed at a particular value of 5.6 mN. We vary its phase ϕ_{m1} at intervals of $\pi/2$ and record the changes in the output spectra, which are illustrated in Fig. 4.

Figure 4(a) illustrates the case when only one of the mechanical driving fields is turned on ($s_{m1} = 5.6$ mN and $s_{m2} = 0$) at a phase of $\phi_{m1} = 3\pi/2$, with Re(η_{as}) reaching its minimum value at the line center, identical to the red curve in Fig. 3(c). Keeping all other parameters fixed, we now change the phase ϕ_{m1} of s_{m1} to $\pi/2$, which gives rise to a sharp increase in Re(η_{as}) at the line center [see Fig. 4(b)], showing remarkable absorptive behavior of the cavity at the $\pi/2$ phase. Other possible interesting values of the phase ϕ_{m1} are explored further. The phase $\phi_{m1} = 0$ results in a Fano-like line shape as shown in Fig. 4(c), and a change in the value of the phase to $\phi_{m1} = \pi$ gives rise to the line shape shown in Fig. 4(d), which is a mirror image of the previous case. Similar features have been observed in other optomechanical systems [66,67]. These results clearly show the importance of the coherent mechanical pump and its phase in controlling the spectral features of the generated fields. The sensitive changes in the behavior of the system, which are detected as a function of the phase of mechanical driving, suggest that this method may be employed as a tool to detect the phase of an unknown harmonic force with considerable precision.

In the above, we have assumed that the oscillation frequencies of both the mirrors are equal to the effective cavity detuning, i.e., $\omega_{m1} = \omega_{m2} = \Omega$, the combination of which was giving rise to resonance at the line center. However, the ability to tune the oscillation frequencies of movable mirrors independently of one another can give rise to asymmetric line shapes as shown in Figs. 5(a) and 5(b). Here we have tuned the oscillation frequency to $\omega_{m1} = 1.2\ \Omega$, due to which the anti-Stokes field will destructively interfere with the probe beam whenever $\omega_{pr} = \omega_{pu} + 1.2\ \Omega$, as shown in Fig. 5(a). We observe the occurrence of a Fano-like resonance and a mirror image of the same, at a corresponding value of 0.2 of the normalized probe detuning, for the phases $\phi_{m1} = 3\pi/2$ and $\phi_{m1} = \pi/2$, respectively. The results presented for various combinations of the mechanical drive fields and their phases show clearly the interference effects between two transition pathways, in this case the fields generated at the probe

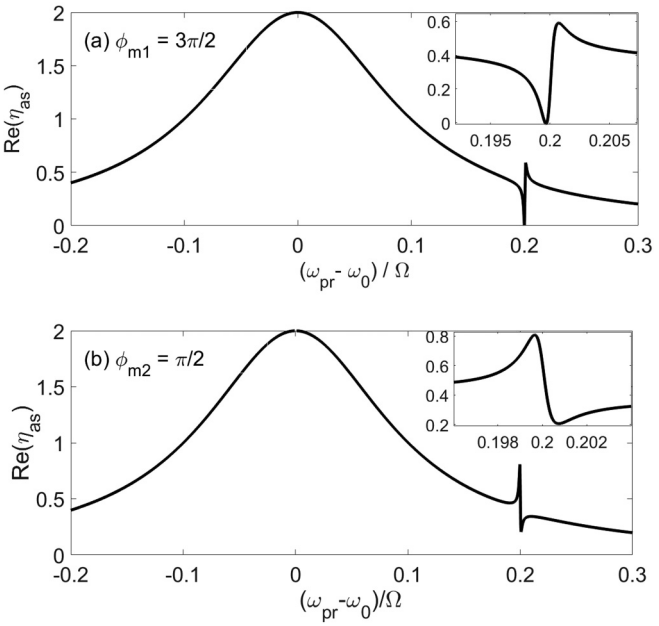

FIG. 5. Fano resonance in the real part of the anti-Stokes field as a function of normalized probe detuning for $s_{m1} = 4.6$ mN and (a) $\phi_{m1} = 3\pi/2$ and (b) $\phi_{m1} = \pi/2$.

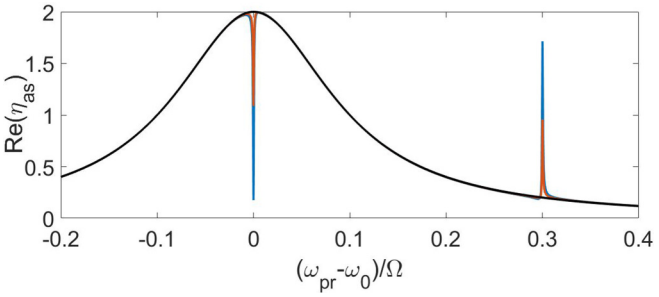

FIG. 6. The real part of the anti-Stokes field as a function of normalized probe detuning $(\omega_{\rm pr} - \omega_0)/\Omega$ for $s_{m1} = 5.2$ mN, $\phi_{m1} = 3\pi/2$ and $s_{m2} = 18$ mN, $\phi_{m2} = \pi$ (blue curve), $s_{m1} = 2.6$ mN, $\phi_{m1} = 3\pi/2$ and $s_{m2} = 9$ mN, $\phi_{m2} = \pi$ (red curve); and $s_{m1} = 0$, $\phi_{m1} = 3\pi/2$ and $s_{m2} = 0$, $\phi_{m2} = \pi$ (black curve).

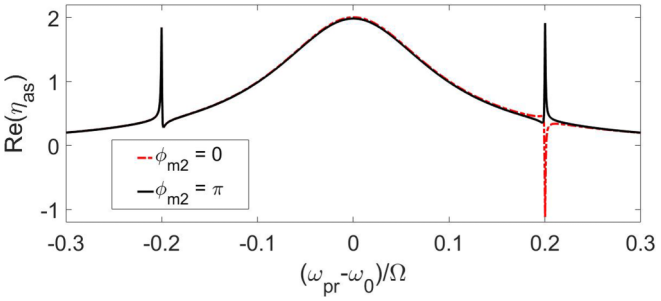

FIG. 7. Double Fano resonance in the real part of the antiStokes field as a function of normalized probe detuning for $s_{m1} = 8$ mN, $\omega_{m1} = 0.8\ \Omega$, $s_{m2} = 12$ mN, $\omega_{m2} = 1.2\ \Omega$, and $\phi_{m1} = \phi_{m2} = 0$ (red dashed curve); and $\phi_{m1} = 0$ and $\phi_{m2} = \pi$ (black solid curve).

frequency and at the anti-Stokes frequency. It is interesting to note that these features have not been observed so far in macroscopic cavities (due to the very weak optomechanical effects in such systems) and are resulting purely due to the introduction of a coherent mechanical driving field(s).

Next, we consider the case when both the mechanical pumps (s_{m1} and s_{m2}) are switched on and degeneracy between oscillation frequencies of the mirrors is removed ($\omega_{m1} \neq \omega_{m2}$). This condition provides two distinct transition pathways [$(\omega_{\rm pu} + \omega_{m1})$ and $(\omega_{\rm pu} + \omega_{m2})$] to interfere with $\omega_{\rm pr}$, which gives rise to two resonances as clearly illustrated in Fig. 6. Here, in addition to the OMIT generated at the line center, a sharp resonance peak at $\delta_{\rm pr}/\Omega = 0.3$ is observed. The parameters considered here are $\omega_{m1} = \Omega$ and $\phi_{m1} = 3\pi/2$, and $\omega_{m2} = \Omega + 0.3\ \Omega$ and $\phi_{m2} = \pi$. Figure 6 clearly shows that the strength (magnitude) of these OM features can be controlled by tuning the amplitude of the mechanical driving field. When $s_{m1} = 5.2$ mN, we see a minima in the generated anti-Stokes field [Re($\eta_{\rm as}$)] at the line center and a maxima at $\delta_{\rm pr}/\Omega = 0.3$ for $s_{m2} = 18$ mN, as shown by the blue curve in Fig. 6. With a decrease in the amplitudes of both mechanical pumps, $s_{m1} = 2.6$ mN and $s_{m2} = 9$ mN, we see a considerable decrease in the strength of resonant curves, as can be seen from the red curve. The black curve illustrates the absence of any OM features as both the mechanical pumps are switched off, i.e., $s_{m1} = s_{m2} = 0$.

We now present our results on double Fano-like resonance line shapes away from the line center, which can be tuned by the introduction of mechanical driving fields and their phases. Such features have been widely studied in a different context in plasmonic structures [68,69]. Very recently, these double Fano resonance line shapes have been studied also in cavity optomechanical systems [35,39,70]. In Fig. 7 the resonant peak and dip on the right of the line center appear due to the introduction of s_{m2} and the peak on the left side results due to the introduction of s_{m1}. The parameters that were considered here are $\omega_{m2} = \Omega + 0.2\ \Omega$ and $\omega_{m1} = \Omega - 0.2\ \Omega$, due to which the resonance due to mirror 1 (s_{m1}) occurs at $\delta_{\rm pr}/\Omega = -0.2$ and that due to mirror 2 (s_{m2}) occurs at $\delta_{\rm pr}/\Omega = 0.2$. These resonances occur due to interference of the probe beam and the anti-Stokes fields that are generated at $\omega_{\rm pu} + \omega_{m1}$ and $\omega_{\rm pu} + \omega_{m2}$, respectively. The location of these peaks can be suitably modified by tuning the mechanical frequency of the movable mirrors. Here, a mechanical pump of $s_{m1} = 8$ mN (Fig. 7) is applied to generate a strong resonance peak on the left, whereas a slightly larger value of s_{m2} (12 mN) is required to generate a resonance peak of similar height on the right side. This asymmetry arises from the fact that the resonance due to s_{m2} occurs when $\omega_{\rm pr} = \omega_{\rm pu} + 1.2\ \Omega$, which is far away from the pump laser frequency as compared to the resonance that occurs due to application of s_{m1} at $\omega_{\rm pr} = \omega_{\rm pu} + 0.8\ \Omega$. Therefore the closer we are to the pump laser frequency $\omega_{\rm pu}$, the smaller is the force that is needed to generate the OM resonance features and vice versa. One observes that by flipping the phase ϕ_{m2} from a value of 0 (red dashed curve) to π (black solid curve), the dip changes to a peak. The negative peak (red dashed curve) at $\delta_{\rm pr}/\Omega = 0.2$ corresponds to resonance amplification which can effectively be shifted to resonance absorption (positive peak) by adjusting the phase (ϕ_{m2}) of the coherent mechanical pump. These features clearly show the important role played by the amplitude and the phase of the coherent mechanical pump in tuning the absorption and amplification features as well as their positions.

Next we consider the case when the mechanical frequency of both oscillators are taken to be equal and tuned away from the effective cavity detuning (Δ) where $\omega_{m1} = \omega_{m2} = 1.3\ \Omega$ where $\Delta = \Omega$, this enables one to control the resonance features by changing the phase of the mechanical pump. When both s_{m1} and s_{m2} have the same phase, namely, $\phi_{m1} = \phi_{m2} = \pi$, they constructively interfere giving rise to resonant enhancement at $\delta_{\rm pr}/\Omega = 0.3$ as shown by the blue curve in Fig. 8. Next, when the relative phase of the mechanical pumps, with strengths $s_{m1} = s_{m2} = 9$ mN, is shifted from π to 2π or 0, destructive interference takes place between the two coherent processes which leads to total cancellation of the Fano-like feature, resulting in the black curve. This situation amounts to effectively turning both the mechanical pumps off. We thus show that by tuning the relative phase between the two mechanical pumps, which are of equal magnitude, we can completely switch on and off the Fano-resonance. Taking their amplitudes unequal will result in further features in the Fano-resonance. For example, the red curve in Fig. 8 corresponds to unequal values of the mechanical driving fields, $s_{m1} = 14$ mN and $s_{m2} = 6$ mN with phases $\phi_{m1} = \pi$ and $\phi_{m2} = 0$, unlike the blue curve, in which both the mechanical drives were taken to have the same amplitude and phase.

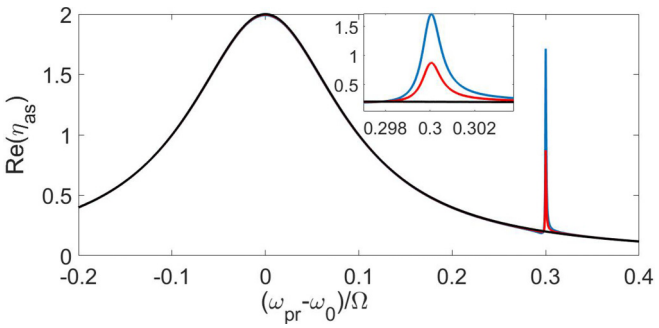

FIG. 8. Real part of anti-Stokes field vs normalized probe detuning for $s_{m1} = s_{m2} = 9$ mN, $\phi_{m1} = \phi_{m2} = \pi$ (blue curve); $s_{m1} = 14$ mN, $\phi_{m1} = \pi$, $s_{m2} = 6$ mN, $\phi_{m2} = 0$ (red curve); $s_{m1} = s_{m2} = 9$ mN, $\phi_{m1} = \pi$, $\phi_{m2} = 0$ (black curve).

IV. CONCLUSION

In this work we have shown how the OM features, viz., the optomechanically induced transparency and asymmetric Fano line shapes can arise in a four-mirror macroscopic optomechanical cavity, due to the inclusion of coherent mechanical driving of the two movable mirrors. In the macroscopic four-mirror optomechanical system considered here, we identify interfering pathways leading to Fano resonances. We further show that these features can be efficiently controlled by changing the phase and the amplitude of mechanical driving. The sensitive changes that are observed in the Fano line shapes with slight modifications in the amplitude and phase of the mechanical driving fields suggests the possibility of exploiting this feature to detect unknown harmonic forces. For the special case of the frequencies of both the mechanical oscillators being equal, it is shown that the phase can be used as a switch to generate interesting optomechanical effects. The freedom of tuning the two mechanical oscillators independently of each other leads to the generation of tunable double Fano-like resonance. In conclusion, this work suggests the possibility of observing interesting tunable quantum effects at macroscopic scales, with the aid of coherent mechanical driving fields.

APPENDIX

The steady-state solutions are given by

$$P_{is} = 0 \quad (i = 1, 2), \quad a_s = \frac{\epsilon_{\rm pu}}{\kappa + i\Delta}, \quad Q_{is} = \frac{G_i |a_s|^2}{\omega_{mi}} \quad (i = 1, 2), \tag{A1}$$

where $\Delta = \Delta_c - G_1 Q_1 - G_2 Q_2$. The equations of motion for the fluctuations in each of the operators are obtained as

$$\left(\frac{d}{dt} + (\kappa + i\Delta_c)\right)\delta a = \epsilon_{\rm pr} e^{-i\delta t} + iG_1(Q_{1s}\delta a + a_s \delta Q_1) + iG_2(a_s \delta Q_2 + Q_{2s}\delta a), \tag{A2}$$

$$\left(\frac{d^2}{dt^2} + \gamma_1 \frac{d}{dt} + \omega_{m1}^2\right)\delta Q_1 = G_1 \omega_{m1}(a_s^* \delta a + a_s \delta a^*) + \frac{S'_{m1}\omega_{m1}}{\hbar}\cos(\delta t + \phi_{m1}), \tag{A3}$$

$$\left(\frac{d^2}{dt^2} + \gamma_2 \frac{d}{dt} + \omega_{m2}^2\right)\delta Q_2 = G_2 \omega_{m2}(a_s^* \delta a + a_s \delta a^*) + \frac{S'_{m2}\omega_{m2}}{\hbar}\cos(\delta t + \phi_{m2}). \tag{A4}$$

We next use the ansatz

$$\delta X_i = X_i^- e^{-i\delta t} + X_i^+ e^{i\delta t} \quad (i = 1, 2) \tag{A5}$$

for each of the variables and substitute this into the equations of motion for the fluctuations and group the coefficients of like terms to obtain the solutions for the relevant quantities of interest:

$$[\kappa + i(\Delta - \delta)]a_1^- = \epsilon_{\rm pr} + iG_1 a_s Q_1^- + iG_2 a_s Q_2^-, \tag{A6}$$

$$[\kappa + i(\Delta + \delta)]a_1^+ = iG_1 a_s Q_1^+ + iG_2 a_s Q_2^+, \tag{A7}$$

$$(\omega_{m1}^2 - i\gamma_1\delta - \delta^2)Q_1^- = G_1\omega_{m1}[a_s^* a_1^- + a_s(a_1^+)^*] + \frac{S'_{m1}\omega_{m1}}{2\hbar}e^{-i\phi_{m1}}, \tag{A8}$$

$$(\omega_{m1}^2 + i\gamma_1\delta - \delta^2)Q_1^+ = G_1\omega_{m1}[a_s^* a_1^+ + a_s(a_1^-)^*] + \frac{S'_{m1}\omega_{m1}}{2\hbar}e^{+i\phi_{m1}}, \tag{A9}$$

$$(\omega_{m2}^2 - i\gamma_2\delta - \delta^2)Q_2^- = G_2\omega_{m2}[a_s^* a_1^- + a_s(a_1^+)^*] + \frac{S'_{m2}\omega_{m2}}{2\hbar}e^{-i\phi_{m2}}, \tag{A10}$$

$$(\omega_{m2}^2 + i\gamma_2\delta - \delta^2)Q_2^+ = G_2\omega_{m2}[a_s^* a_1^+ + a_s(a_1^-)^*] + \frac{S'_{m2}\omega_{m2}}{2\hbar}e^{+i\phi_{m2}}, \tag{A11}$$

the solutions of which are obtained as

$$Q_2^- = \frac{\epsilon_{\rm pr} c_s^* G_2 \chi_2(\delta)\alpha + 2\Delta\chi_2(\delta) G_1 G_2 |c_s|^2 Q_1^- + S_{m2}\chi_2(\delta)\alpha\beta e^{-i\phi_{m2}}}{\alpha\beta - 2G_2^2|c_s|^2\chi_2(\delta)\Delta}, \tag{A12}$$

$$Q_1^- = \frac{\alpha\chi_1(\delta)\{\epsilon_{\rm pr} c_s^* G_1[d_2 + 2\Delta G_2^2|c_{2s}|^2\chi_2(\delta)] + \beta S_{m1} e^{-i\phi_{m1}} d_2\} + \alpha\beta\chi_1(\delta)\chi_2(\delta) 2\Delta G_1 G_2 |c_{2s}|^2 S_{m2} e^{-i\phi_{m2}}}{d_1 d_2 - 4\Delta^2 G_1^2 G_2^2 |c_s|^4 \chi_1(\delta)\chi_2(\delta)}, \tag{A13}$$

$$a_1^- = \frac{\epsilon_{\rm pr} + iG_1 a_s Q_1^- + iG_2 a_s Q_2^-}{\kappa + i(\Delta - \delta)}. \tag{A14}$$

Each of the hitherto undefined quantities that appear in the above solutions are defined by

$$\alpha = [\kappa - i(\Delta + \delta)], \quad \beta = [\kappa + i(\Delta - \delta)], \quad d_1 = \alpha\beta - 2G_1^2|c_s|^2\chi_1(\delta)\Delta, \quad d_2 = \alpha\beta - 2G_2^2|c_s|^2\chi_2(\delta)\Delta,$$
$$\Delta = \Delta_c - G_1 Q_1 - G_2 Q_2, \quad S_{mi} = \frac{S'_{mi}}{2\hbar}\ (i = 1, 2), \quad \chi_1(\delta) = \frac{\omega_{m1}}{\omega_{m1}^2 - i\gamma_1\delta - \delta^2}, \quad \text{and} \quad \chi_2(\delta) = \frac{\omega_{m2}}{\omega_{m2}^2 - i\gamma_2\delta - \delta^2}. \tag{A15}$$

[1] U. Fano, Phys. Rev. **124**, 1866 (1961).
[2] A. R. P. Rau, Phys. Scr. **69**, C10-13 (2004).
[3] J. F. Scott, Rev. Mod. Phys. **46**, 83 (1974).
[4] M. Hase, J. Demsar, and M. Kitajima, Phys. Rev. B **74**, 212301 (2006).
[5] J. Faist, F. Capasso, C. Sitori, K. W. West, and L. N. Pfeiffer, Nature (London) **390**, 589 (1997).
[6] M. Kroner, A. O. Govorov, S. Remi, B. Biedermann, S. Seidl, A. Badolato, P. M. Petroff, W. Zhang, R. Barbour, B. D. Gerardot, R. J. Warburton, and K. Karrai, Nature (London) **451**, 311 (2008).
[7] B. Gunupudi, S. R. Das, R. Navarathna, S. K. Sahu, S. Majumder, and V. Singh, Phys. Rev. Appl. **11**, 024067 (2019).
[8] S. Fan, Appl. Phys. Lett. **80**, 908 (2002).
[9] D. D. Smith, H. Chang, K. A. Fuller, A. T. Rosenberger, and R. W. Boyd, Phys. Rev. A **69**, 063804 (2004).
[10] B. Luk'yanchuk, N. I. Zheludev, S. A. Maier, N. J. Halas, P. Nordlander, H. Giessen, and C. T. Chong, Nat. Mater. **9**, 707 (2010).
[11] N. Liu, L. Langguth, T. Weiss, J. Kästel, M. Fleischhauer, T. Pfau, and H. Giessen, Nat. Mater. **8**, 758 (2009).
[12] Y. Yoon, M. G. Kang, T. Morimoto, M. Kida, N. Aoki, J. L. Reno, Y. Ochiai, L. Mourokh, J. Fransson, and J. P. Bird, Phys. Rev. X **2**, 021003 (2012).
[13] S. Sasaki, H. Tamura, T. Akazaki, and T. Fujisawa, Phys. Rev. Lett. **103**, 266806 (2009).
[14] A. C. Johnson, C. M. Marcus, M. P. Hanson, and A. C. Gossard, Phys. Rev. Lett. **93**, 106803 (2004).
[15] K. Kobayashi, H. Aikawa, A. Sano, S. Katsumoto, and Y. Iye, Phys. Rev. B **70**, 035319 (2004).
[16] M. V. Rybin, A. B. Khanikaev, M. Inoue, K. B. Samusev, M. J. Steel, G. Yushin, and M. F. Limonov, Phys. Rev. Lett. **103**, 023901 (2009).
[17] M. Rahmani, D. Y. Lei, V. Giannini, B. Lukiyanchuk, M. Ranjbar, T. Y. F. Liew, M. Hong, and S. A. Maier, Nano Lett. **12**, 2101 (2012).
[18] W. Ding, B. Luk'yanchuk, and C. W. Qiu, Phys. Rev. A **85**, 025806 (2012).
[19] S. Nojima, M. Usuki, M. Yawata, and M. Nakahata, Phys. Rev. A **85**, 063818 (2012).
[20] G. L. Shang, G. T. Fei, Y. Zhang, P. Yan, S. H. Xu, H. M. Ouyang, and L. D. Zhang, Sci. Rep. **4**, 3601 (2014).
[21] B. Gallinet and O. J. F. Martin, ACS Nano **5**, 8999 (2011); Phys. Rev. B **83**, 235427 (2011); Y. Francescato, V. Giannini, and S. A. Maier, ACS Nano **6**, 1830 (2012); A. Artar, A. Ali Yanik, and H. Altug, Nano Lett. **11**, 3694 (2011); R. Taubert, M. Hentschel, J. Kastel, and H. Giessen, *ibid.* **12**, 1367 (2012).
[22] N. Verellen, Y. Sonnefraud, H. Sobhani, F. Hao, V. V. Moshchalkov, P. Van Dorpe, P. Nordlander, and S. A. Maier, Nano Lett. **9**, 1663 (2009).
[23] A. E. Miroshnichenko, S. Flach, and Y. S. Kivshar, Rev. Mod. Phys. **82**, 2257 (2010).
[24] J. Ye, F. Wen, H. Sobhani, J. B. Lassiter, P. V. Dorpe, P. Nordlander, and N. J. Halas, Nano Lett. **12**, 1660 (2012).
[25] C. Wu, A. B. Khanikaev, and G. Shvets, Phys. Rev. Lett. **106**, 107403 (2011).
[26] Z. K. Zhou, X. N. Peng, Z. J. Yang, Z. S. Zhang, M. Li, X. R. Su, Q. Zhang, X. Shan, Q. Q. Wang, and Z. Zhang, Nano Lett. **11**, 49 (2011).
[27] K. L. Lee, S. H. Wu, C. W. Lee, and P. K. Wei, Opt. Express **19**, 24530 (2011).
[28] A. Xuereb, R. Schnabel, and K. Hammerer, Phys. Rev. Lett. **107**, 213604 (2011).
[29] V. G. Arkhipkin and Y. I. Heller, Phys. Lett. A **98**, 12 (1983).
[30] O. A. Kocharovskaya and Ya. I. Khanin, Pis'ma Zh. Eksp. Teor. Fiz. **48**, 581 (1988) [JETP Lett. **48**, 630 (1988)].
[31] M. O. Scully, S. Y. Zhu, and A. Gavrielides, Phys. Rev. Lett. **62**, 2813 (1989).
[32] E. S. Fry, X. Li, D. Nikonov, G. G. Padmabandu, M. O. Scully, A. V. Smith, F. K. Tittel, C. Wang, S. R. Wilkinson, and S. Y. Zhu, Phys. Rev. Lett. **70**, 3235 (1993).
[33] G. S. Agarwal, S. L. Haan, and J. Cooper, Phys. Rev. A **29**, 2552 (1984).
[34] A. Barnthaler, S. Rotter, F. Libisch, J. Burgdorfer, S. Gehler, U. Kuhl, and H. J. Stockmann, Phys. Rev. Lett. **105**, 056801 (2010).
[35] K. Qu and G. S. Agarwal, Phys. Rev. A **87**, 063813 (2013).
[36] S. Zhang, J. Li, R. Yu, W. Wang, and Y. Wu, Sci Rep. **7**, 39781 (2017).

[37] M. J. Akram, F. Ghafoor, M. M. Khan, and F. Saif, Phys. Rev. A **95**, 023810 (2017).
[38] K. A. Yasira and W. M. Liu, Sci. Rep. **6**, 22651 (2016).
[39] C. Jiang, L. Jiang, H. Yu, Y. Cui, X. Li, and G. Chen, Phy. Rev. A **96**, 053821 (2017).
[40] M. J. Akram, F. Ghafoor, and F. Saif, J. Phys. B **48**, 065502 (2015).
[41] M. Abbas, R. Ullah, Y. L. Chuang, and Ziauddin, J. Mod. Opt. **66**, 176 (2018).
[42] X. Piao, S. Yu, S. Koo, K. Lee, and N. Park, Opt. Express **19**, 10907 (2011).
[43] X. Piao, S. Yu, and N. Park, Opt. Express **20**, 18994 (2012).
[44] X. Piao, S. Yu, J. Hong, and N. Park, Sci. Rep. **5**, 16585 (2015)
[45] A. H. Safavi-Naeini, T. P. M. Alegre, J. Chan, M. Eichenfield, M. Winger, Q. Lin, J. T. Hill, D. E. Chang, and O. Painter, Nature (London) **472**, 69 (2011).
[46] F. Elste, S. M. Girvin, and A. A. Clerk, Phys. Rev. Lett. **102**, 207209 (2009).
[47] C. Min and G. Veronis, Opt. Express **17**, 10757 (2009).
[48] K. Kobayashi, H. Aikawa, S. Katsumoto, and Y. Iye, Phys. Rev. Lett. **88**, 256806 (2002).
[49] S. Weis, R. Riviére, S. Deléglise, E. Gavartin, O. Arcizet, A. Schliesser, and T. J. Kippenberg, Science **330**, 1520 (2010).
[50] P. Fritschel, M. Evans, and V. Frolov, Opt. Express **22**, 4224 (2014).
[51] F. Farman and A. Bahrampour, *Research in Optical Science*, OSA Technical Digest (online) (Optical Society of America, 2014), paper JW2A.44.
[52] B. Teklu, T. Byrnes, and F. S. Khan, Phys. Rev. A **97**, 023829 (2018).
[53] W. Ge, M. Al-Amri, H. Nha, and M. S. Zubairy, Phys. Rev. A **88**, 052301 (2013).
[54] G. S. Agarwal, *Quantum Optics* (Cambridge University, Cambridge, England, 2013).
[55] K. C. Yellapragada, N. Pramanik, S. Singh, and P. A. Lakshmi, Phys. Rev. A **98**, 053822 (2018).
[56] P. Sekatski, M. Aspelmeyer, and N. Sangouard, Phys. Rev. Lett. **112**, 080502 (2014).
[57] S. Mancini, D. Vitali, and P. Tombesi, Phys. Rev. Lett. **80**, 688 (1998); D. Vitali, S. Mancini, L. Ribichini, and P. Tombesi, J. Opt. Soc. Am. B **20**, 1054 (2003).
[58] L. F. Buchmann, L. Zhang, A. Chiruvelli, and P. Meystre, Phys. Rev. Lett. **108**, 210403 (2012).
[59] J. Q. Liao, Q. Q. Wu, and F. Nori, Phys. Rev. A **89**, 014302 (2014); H. Tan, F. Bariani, G. Li, and P. Meystre, *ibid.* **88**, 023817 (2013); S. Mancini, V. Giovannetti, D. Vitali, and P. Tombesi, Phys. Rev. Lett. **88**, 120401 (2002).
[60] T. P. Purdy, R. W. Peterson, and C. A. Regal, Science **339**, 801 (2013).
[61] F. Mueller, S. Heugel, and L. J. Wang, Phys. Rev. A **79**, 031804(R) (2009).
[62] J. T. Santos, J. Li, J. Ilves, C. F. Ockeloen-Korppi, and M. Sillanpää, New J. Phys. **19**, 103014 (2017).
[63] N. Matsumoto, K. Komori, Y. Michimura, G. Hayase, Y. Aso, and K. Tsubono, Phys. Rev. A **92**, 033825 (2015).
[64] H. Suzuki, E. Brown, and R. Sterling, Phys. Rev. A **92**, 033823 (2015).
[65] J. W. Yoon and R. Magnusson, Opt. Express **21**, 17759 (2013).
[66] J. Ma, C. You, L. Gang Si, H. Xiong, J. Li, X. Yang, and Y. Wu, Sci. Rep. **5**, 11278 (2015).
[67] W. Z. Jia, L. F. Wei, Yong Li, and Y.-x. Liu, Phys. Rev. A **91**, 043843 (2015).
[68] J. Wang, C. Fan, J. He, P. Ding, E. Liang, and Q. Xue, Opt. Express **21**, 2236 (2013).
[69] B. Dana and A. Bahabad, Opt. Express **24**, 22334 (2016).
[70] A. Sohail, Y. Zhang, G. Bary, and C. Shui Yu, Int. J. Theor. Phys. **57**, 2814 (2018).